ELSEVIER

Catalysis Today 82 (2003) 41–48

CATALYSIS TODAY

www.elsevier.com/locate/cattod

A photocatalytic membrane reactor for gas-phase reactions using porous titanium oxide membranes

Toshinori Tsuru*, Takehiro Kan-no, Tomohisa Yoshioka, Masashi Asaeda

Department of Chemical Engineering, Hiroshima University, Higashi-Hiroshima 739-8527, Japan

Abstract

Photocatalytic membrane reactors using porous titanium oxide membranes having pore sizes of several nanometers were utilized for a gas-phase reaction of methanol. Air mixed with methanol (MeOH) vapor, the concentration of which was controlled in the range of 500–6000 ppm, was fed to the photocatalytic membrane reactor in the range of 50–500 cm^3/min using several types of flow patterns. Photocatalysis with membrane permeation resulted in a large decomposition rate, compared to photocatalysis without membrane permeation. The characteristics of the reaction such as decomposition ratio of MeOH, the conversion of the decomposed MeOH to CO_2 and H_2O were found to be a function of the residence time in the reactor. The photocatalytic reaction was analyzed based on pseudo-first-order kinetics to ascertain its simplicity, and the fitted curves were found to be in a relatively good agreement with the experimental data. Apparent rate constants with and without membrane permeation were 2.5 and 1.5×10^{-6} m s^{-1}, respectively, indicating that the performance of the photocatalytic reaction system with membrane permeation was enhanced.

Keywords: Titanium oxide; Photocatalysis; Membrane reactor; Methanol; Porous membrane

1. Introduction

Photocatalytic reactions using titanium oxide (TiO_2), based on the photogeneration of OH radicals by positive photoholes by ultraviolet irradiation and subsequent oxidation reactions, has been extensively investigated either in the form of powders or pellets [1]. The performance of immobilized TiO_2 catalysts in the form of TiO_2 films on nonporous substrates such as glass tube [1,2] or grafting monomers blended with TiO_2 powder on porous polyester supports [3], has been reported. Dijkstra et al. [4] compared several types of photocatalytic reactors including a powder-suspended system, a packed-bed reactor composed of TiO_2-coated glass beads, and a tubular type reactor with a TiO_2 catalyst coated on the wall. Another approach to immobilize TiO_2 powders is to combine a TiO_2 slurry with membrane filtration; in this system, the polymeric membranes were used as a separating layer to retain the catalyst [5].

The strategy used in this study was to utilize porous TiO_2 membranes having pores of several nanometers, that is, a new type of photocatalytic reaction system in which the titanium dioxide itself is immobilized in the form of a porous membrane which is capable of not only selective permeation but also a photocatalytic reaction [6,7], as shown in Fig. 1. The oxidation reaction occurs both on the surface and inside the porous TiO_2 membranes. The advantages of the system are (1) the forced transport of reactants by convection to the TiO_2 membranes, (2) the oxidation reaction on the outer and inner surface of the porous TiO_2 membranes

* Corresponding author. Tel.: +81-824-247-714; fax: +81-824-245-494.
E-mail address: tsuru@hiroshima-u.ac.jp (T. Tsuru).

0920-5861/$ – see front matter © 2003 Elsevier B.V. All rights reserved.
doi:10.1016/S0920-5861(03)00200-1

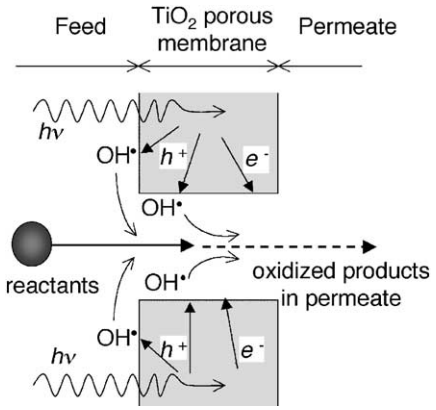

Fig. 1. Schematic concept for photocatalytic membrane reactor.

where high concentrations of OH radicals would be expected, and (3) the potential for obtaining a permeate stream oxidized with OH radicals after a one-pass permeation through the TiO_2 membranes.

From the viewpoints of reaction phases and types of reactants, photocatalytic reactions have been investigated in the liquid phase [1–8] as well as in the gas phase [9–11]. The decomposition of environmental pollutants such as trichloroethylene (TCE) via photocatalytic reactions [1–3,10,11], has been examined, as well as formaldehyde and acetaldehyde [4,9], and phenol [5]. Overall photocatalysis by TiO_2 has been achieved through several independent processes: transfer of reactant in bulk to the surface, adsorption of reactant, reaction in the adsorbed phase, and desorption [1]. The transport of organic compounds through a boundary layer on a TiO_2 surface, which is a relatively slow process in the liquid phase, compared with in the gas phase, could be a rate-determining step in the overall decomposition rate [12], and therefore, the enhanced activity by photocatalytic membrane reactors has been proposed and verified by the decomposition of TCE in the liquid phase [6,7], and would be expected for gas-phase reaction as well.

In the present study, TiO_2 membranes having pore sizes of several nanometers were fabricated and investigated for use in the gas-phase photocatalytic reaction of methanol as a model volatile organic component (VOC). The reaction rate using the photocatalytic membrane reactor was compared with that without membrane permeation at various reaction conditions (residence time, feed concentration).

2. Experimental

Porous TiO_2 membranes were prepared by coating colloidal TiO_2 sols, prepared by hydrolysis and condensation reaction of titanium *iso*-propoxide or commercially available (STS01, kindly supplied by Ishihara Sangyo Kaisha, Japan), on the outer surface of cylindrical α-alumina microfiltration membranes (length 9 cm; outer diameter 1 cm; average pore diameter 1 μm), followed by firing at 450 °C. Both ends of the cylindrical α-alumina microfiltration membranes were connected to glass tubes; one end of which was sealed, while the other end was used for the permeate stream [6,7,13,14]. The average pore size distribution of a TiO_2 membrane used in the present study was approximately 6.5 nm, as shown in Appendix A.

Four blacklight (BL) lamps (4 W, main wavelength 350 nm) were mounted outside the membrane cell unit, the outer housing of which was made of quartz tubing (inner diameter 19 mm, thickness 1 mm). The light intensity at the membrane surface was 4.2 mW/cm^2, as determined by a BL radiometer with an aid of optical fibers. Air from a gas cylinder, was mixed with methanol (MeOH) supplied by a syringe pump, and the resulting mixture was heated to vaporize the MeOH before entering the reactor. The MeOH concentration was controlled in the range of 500–6000 ppmw and the feed flow rate to the photocatalytic membrane reactor was in the range of 50–500 cm^3/min. Three types of flow patterns, schematically shown in Fig. 2, were examined. The temperature of the TiO_2 membrane was maintained at approximately 100 °C by BL irradiation through radiation heat transfer as well as heat release by the recombination of photoholes and electrons generated

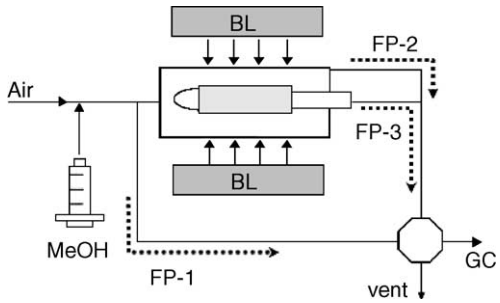

Fig. 2. Schematic experimental photocatalytic reactor and flow patterns used for the photocatalytic reaction.

by the adsorption of photons. The pressure of the feed stream was approximately 10 and 50 kPa, for the case of flow patterns, FP-2 and FP-3, respectively, under a feed flow rate of 500 cm^3/min. Gas compositions were determined by gas chromatography using a thermal conductive detector (TCD-GC: Shimadzu GC 14BT) with TCD current of 150 mA. The temperature of the packed column (Porapak T, length 2 m) was controlled at 135 °C for the analysis of methanol and H_2O, while it was decreased to 100 °C for the analysis of CO_2. A sample volume of 5 cm^3 was introduced through a six-way valve to the on-line GC, which was employed for quantitative analysis of methanol, water and CO_2, and for qualitative analysis of formaldehyde, formic acid, and methylformate as intermediate products.

3. Results and discussion

3.1. Photocatalytic membrane reactor for methanol oxidation

The time course for MeOH concentrations is shown in Fig. 3 for the case of a feed flow rate, Q_F, of 500 cm^3/min. In the FP-1 flow pattern, where the feed gas by-passed the photocatalytic reactor, the MeOH concentration, $C_{MeOH,in}$, was adjusted to approximately 1000 ppm (weight basis). After changing the flow pattern from FP-1 to FP-2, where the feed gas flowed out from the reactor without membrane permeation, the MeOH concentration was reduced to 850 ppm under BL irradiation, while the MeOH concentration was reduced to 700 ppm in the case of FP-3 where all the feed gas permeated the TiO_2 membrane. It should be noted that the MeOH concentration in FP-3, after switching off the BL lamps, returned to the level of feed concentration which was adjusted to approximately 1000 ppm in FP-1. It is obvious that MeOH was decomposed by photocatalysis. The CO_2 concentration, which was approximately 300 ppm in the case of FP-1 and approximately the same level of average concentration contained in atmosphere, increased only slightly, by less than 50 ppm, by the photocatalytic reaction in FP-2 and FP-3. On the other hand, the H_2O concentration increased from 600 ppm, which was contained in the compressed air cylinder, to 900 ppm after the photocatalysis of methanol. It

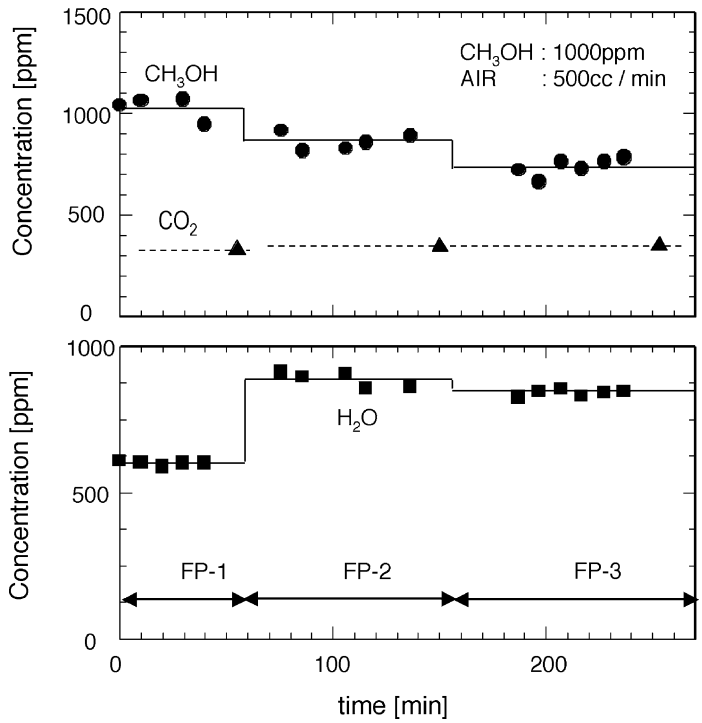

Fig. 3. Time course for the concentration of MeOH, CO_2, and H_2O for three types of flow patterns ($Q_F = 500\ cm^3$/min, $C_{in} \approx 1000$ ppm).

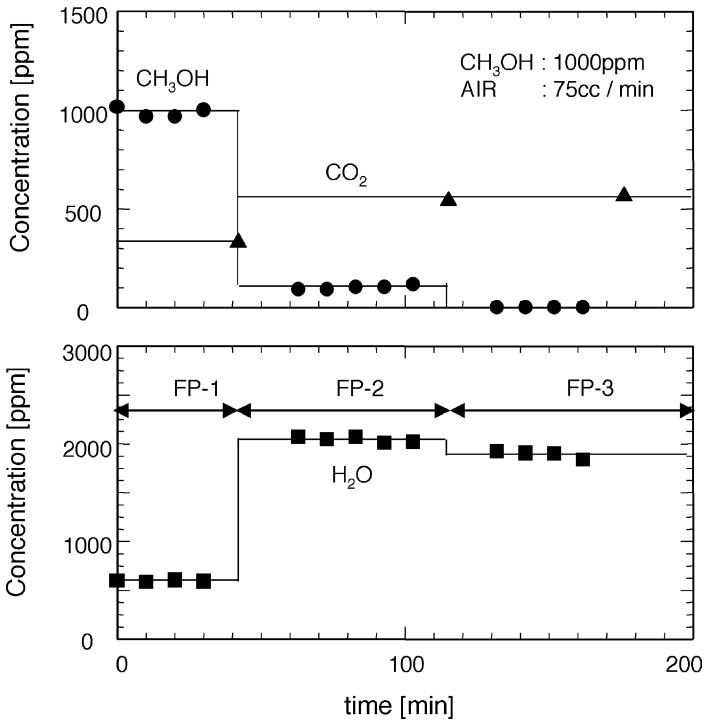

Fig. 4. Time course for the concentration of MeOH, CO_2, and H_2O for three types of flow patterns ($Q_F = 75\,cm^3/min$, $C_{in} \approx 1000\,ppm$).

appears that H_2O concentration in FP-2 is slightly larger than that in FP-3. The time course for MeOH concentration for the case of a flow rate of $75\,cm^3/min$ is shown in Fig. 4. Methanol was decomposed to 100 ppm for the case of FP-2, and almost completely for FP-3. The CO_2 and H_2O concentrations increased drastically as the result of the photocatalytic reaction because of the large decomposition ratio of MeOH.

3.2. Comparison of photocatalytic reaction with and without membrane

Reaction performances were dependent on the types of flow patterns: FP-2 (without membrane permeation) and FP-3 (with membrane permeation), as shown in Figs. 3 and 4. Fig. 5(a)–(c) show MeOH concentrations at the outlet of the photocatalytic membrane reactor, $C_{MeOH,out}$, the decomposition ratio of MeOH, defined as $1 - C_{MeOH,out}/C_{MeOH,in}$, and the decomposition rate, for the case of a MeOH feed concentration, $C_{MeOH,in}$, of approximately 1000 ppm. Fig. 5(d) and (e) show the rate of production of CO_2 and H_2O. At a Q_F of $50\,cm^3/min$, MeOH was decomposed completely for both FP-2 and FP-3, and the decomposition ratio decreased with an increase in Q_F, because of a decrease in residence time in the photocatalytic reaction zone. The photocatalytic reaction with membrane permeation, which was achieved by choosing flow pattern FP-3, shows a larger decomposition ratio and decomposition rate than the case for the photocatalytic reaction without membrane permeation (FP-2), which corresponds to a conventional photocatalytic reactor composed of a thin TiO_2 film prepared on nonporous substrates. For the case of the photocatalytic reaction with membrane permeation, all reactants were required to permeate through TiO_2 pores of several nanometers, providing for more effective contact between the reactants and the catalytically active TiO_2 surface. That is, the membrane permeation system provided a uniform residence time for the reaction. Moreover, the transport of organic compounds to the surface of the TiO_2 was enhanced

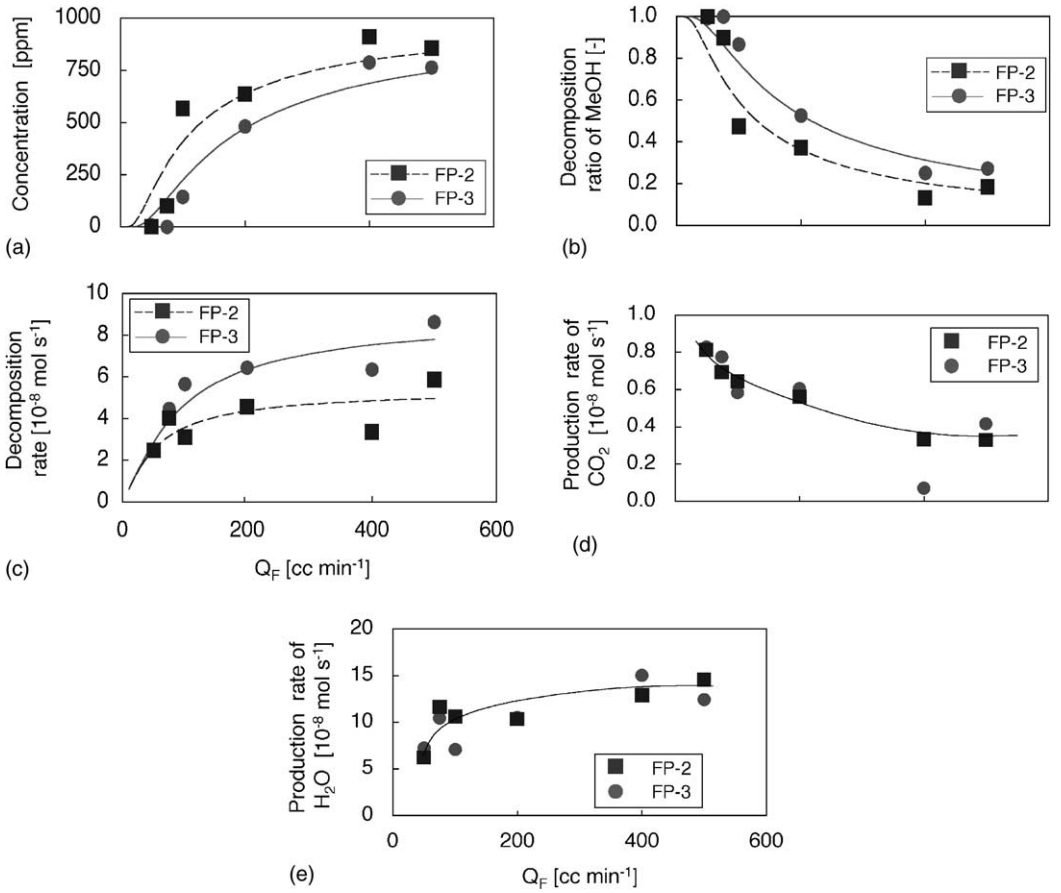

Fig. 5. Photocatalytic reaction performances as a function of feed flow rate, Q_F, for the flow pattern, FP-2 (without membrane permeation) and FP-3 (with membrane permeation): (a) MeOH concentration in the outlet; (b) MeOH decomposition ratio; (c) MeOH decomposition rate; (d) production rate of CO_2; (e) production rate of H_2O ($C_{in} \approx 1000$ ppm).

by forced convection in addition to transport by diffusion, and a larger surface area could be utilized for the photocatalytic reaction with membrane permeation.

The decomposition rate of MeOH increased with an increase in air flow rate, and then appears to level off. This can be explained as follows; since the MeOH feed concentration was maintained at approximately 1000 ppm, by increasing the air feed flow rate, the MeOH feed flow rate was also increased and the decomposition rate of MeOH was limited, probably by the amount of BL irradiation and/or the reduced residence time in the photocatalytic reactor. In terms of products of methanol decomposition, the rate of production of H_2O increased with Q_F, and no obvious difference between photocatalytic reactions with and without membrane permeation was observed. Assuming that 1 mole of OH radicals, generated by 1 mole of photons, can produce 1 mole of water molecules by reaction with organic compounds, it can be concluded that the amounts of OH radicals were the same, irrespective of flow patterns. This appears to be in reasonable agreement with the saturated H_2O generation rate shown in Fig. 5(e). On the other hand, CO_2 generated by the photocatalytic reaction decreased with an increase in air flow rate.

Fig. 6 indicates the ratio of CO_2 production rate to the MeOH decomposition rate by photocatalytic reactions with and without membrane permeation, calculated from the data of Fig. 5. It is clear that MeOH was

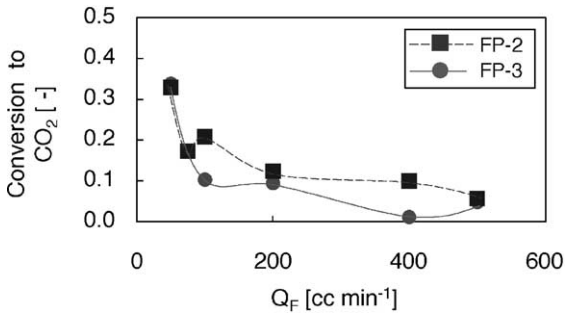

Fig. 6. Conversion of decomposed MeOH to CO_2 by a photocatalytic reaction for the flow pattern, FP-2 (without membrane permeation) and FP-3 (with membrane permeation).

not completely decomposed to CO_2, and that the ratio of the CO_2 production rate to the MeOH decomposition rate, that is, the conversion of the decomposed MeOH to CO_2, ranged approximately from 10 to 30%, probably because the photocatalytic reactions in the present study were carried out under an extremely dilute H_2O concentration. Photocatalytic reactions in the gas phase have been explained by the adsorption of organic components to the TiO_2 surface and subsequent oxidation reaction by OH radicals which are generated by the oxidation of adsorbed water. The oxidation of MeOH occurs in a consecutive reaction manner where MeOH is oxidized to formaldehyde, formic acid, and finally CO_2 and all of these components were detected by GC analysis quantitatively for MeOH and CO_2, and qualitatively for formaldehyde. Another possible reaction path, that is, an esterification reaction between methanol and formic acid has also been suggested, since the presence of methylformate was detected qualitatively by GC analysis. The relatively low conversion to CO_2 might be explained by production of a large mount of intermediates. Another point, which should be addressed, is the dependency on feed flow rate, Q_F. The conversion to CO_2 appears to increase with a decrease in Q_F, probably because of the longer residence time in the photocatalytic reaction zone, which caused the complete oxidation of methanol.

Fig. 7 shows the effect of feed concentration of MeOH at a constant air flow rate of 500 cm^3/min. The decomposition ratio decreased with feed concentration, while the decomposition rate of MeOH increased and appears to reach a constant value. This

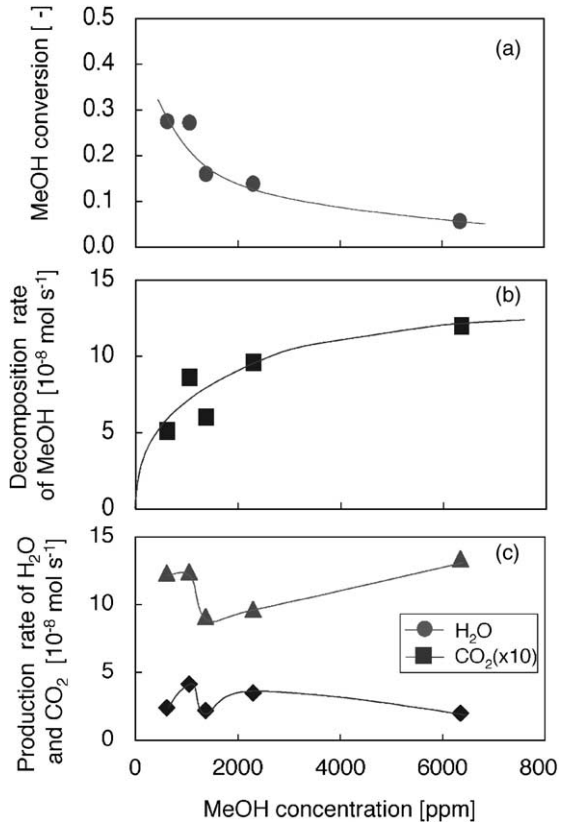

Fig. 7. Effect of feed concentration of MeOH on (a) MeOH decomposition ratio, (b) the decomposition rate of MeOH, and (c) production rate of CO_2 and water (with membrane permeation, air flow rate of 500 cm^3/min.)

is probably because the reaction rate is limited by the Langmuir–Hinshelwood mechanism where the reaction is first-order at low concentrations and zero-order at high concentrations. On the other hand, the CO_2 and H_2O production rates appear to be independent of feed concentration. Consequently, the conversion of decomposed MeOH to CO_2 and H_2O decreased with an increase in MeOH concentration, suggesting that more intermediates were produced at high concentration.

In summary, it can be concluded that photocatalysis with membrane permeation shows a large decomposition rate for MeOH, compared with photocatalysis without a membrane. The characteristics of the reaction such as decomposition ratio can be controlled by the residence time in photocatalytic membrane reactor.

3.3. Pseudo-first-order analysis of gas-phase oxidation of methanol in catalytic membrane reactor

In this section, pseudo-first-order reaction kinetics are also applied to evaluate photocatalytic performance with and without membrane permeation, based on the advantage of simplicity, although the photocatalytic reaction has also been analyzed by Langmuir–Hinshelwood mechanism. In flow patterns FP-2 and FP-3, MeOH was decomposed from inlet concentration, C_{in}, to outlet concentration, C_{out}, during a given residence time. For the case of FP-2 where methanol with an inlet concentration of C_{in} was decomposed on the TiO_2 membrane surface and flowed out at C_{out}. By assuming a plug-flow model and an apparent pseudo-first-order reaction constant, $k_{FP\text{-}2}$, the following equation can be derived:

$$\ln\left(\frac{C_{out}}{C_{in}}\right) = -\frac{k_{FP\text{-}2}}{Q_F} \quad (1)$$

For the case of FP-3, C_{in} and C_{out} were assumed to be the concentrations of feed and permeate for the TiO_2 membrane, respectively, and complete mixing was assumed in the membrane reactor, that is, MeOH concentration in feed was uniform at C_{in}. Therefore, the decomposition reaction was assumed to occur during the permeation of the TiO_2 pores in a plug-flow manner, with an apparent rate constant, $k_{FP\text{-}3}$, and therefore, the same equation can be utilized:

$$\ln\left(\frac{C_{out}}{C_{in}}\right) = -\frac{k_{FP\text{-}3}}{Q_F} \quad (2)$$

As shown in Fig. 8, $k_{FP\text{-}2}$ and $k_{FP\text{-}3}$, the apparent reaction rate constants for a pseudo-first-order reaction based on Eqs. (1) and (2), decreased drastically in low concentrations, and appears to approach a constant value. This can be explained by the Langmuir–Hinshelwood mechanism where the apparent first-order reaction rate constant shows larger values at low concentration and decreases with an increase in concentration. At a low Q_F, methanol was almost completely decomposed as shown in Fig. 5, leading to a larger rate constant at low concentration.

The curves shown in Fig. 5(a)–(c), which were calculated using the averaged rate constants, are in relatively good agreement with the experimental data. Reaction constants for the case of the photocatalytic reaction with and without membrane permeation, $k_{FP\text{-}3}$ and $k_{FP\text{-}2}$, were 2.5 and $1.5 \times 10^{-6}\,m\,s^{-1}$, respectively, indicating an enhanced performance of the photocatalytic reaction system with membrane permeation.

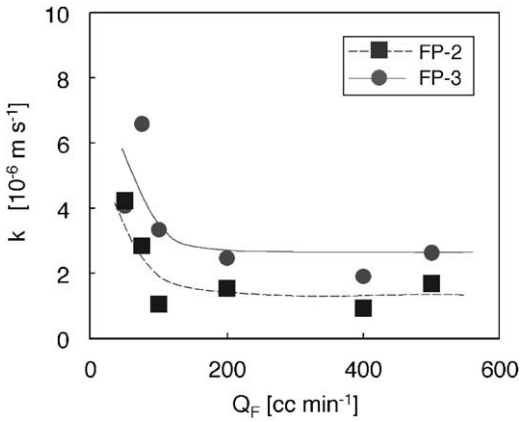

Fig. 8. Apparent reaction rate constants obtained by assuming pseudo-first-order reaction kinetics for the photocatalytic reaction with (FP-3) and without membrane permeation (FP-2).

4. Conclusions

A photocatalytic membrane reactor using porous titanium oxide membranes having pore sizes of several nanometers was applied to the gas-phase oxidation of methanol. Air mixed with methanol (MeOH) vapor, the concentration of which was controlled in the range of 500–6000 ppm, was fed to the photocatalytic membrane reactor in the range of 50–500 cm^3/min in various types of flow patterns. Photocatalysis with membrane permeation shows a large decomposition rate, in comparison with photocatalysis without membrane permeation. The reaction characteristics such as decomposition ratio, conversion to CO_2 and H_2O can be controlled by the residence time in the photocatalytic membrane reactor. The photocatalytic reaction was analyzed based on pseudo-first-order reaction kinetics for simplicity, and the fitted curves were found to be in relatively good agreement with the experimental data. Apparent rate constants with and without membrane permeation were 2.5 and $1.5 \times 10^{-6}\,m\,s^{-1}$, respectively, indicating an enhanced performance of photocatalytic reaction system with membrane permeation.

Appendix A

In this section, the pore size distribution of a porous TiO_2 membrane, which was determined by nanopermporometry, is shown in Fig. 9. In the case of nanopermporometry where a mixture of a noncondensable gas such as N_2 and a condensable gas (vapor) such as H_2O is fed to the porous membranes and the permeability of the noncondensable gas is measured, the vapor is assumed to be capillary-condensed in membranes pores smaller than the following Kelvin diameter, d_K, and to block the permeation of a noncondensable gas.

$$d_K = -\frac{4\bar{v}\sigma\cos\theta}{RT\ln(P/P_s)}$$

where θ is the contact angle, σ the surface tension, v the molar volume, P the vapor pressure, and P_s is the saturation vapor pressure.

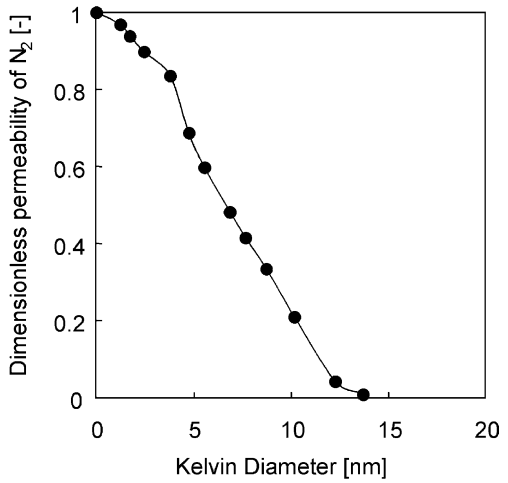

Fig. 9. Dimensionless permeability of nitrogen as a function of Kelvin diameter (TiO_2 membrane).

The dimensionless permeability of nitrogen (DPN), which is normalized with the permeability of pure nitrogen, is plotted as a function of Kelvin diameter. The pore size distribution can be estimated based on the DPN curve, indicating the average pore size determined by 50% of DPN is 6.5 nm as shown in the figure. Details of the experimental apparatus can be found in our previous paper [15].

References

[1] J.M. Herrmann, Catal. Today 53 (1999) 115.
[2] R.W. Matthews, J. Phys. Chem. 91 (1987) 3328.
[3] I.R. Bellobono, B. Barni, F. Gianturco, J. Membr. Sci. 102 (1995) 139.
[4] M.F.J. Dijkstra, H. Buwalda, A.W.F. de Jong, A. Michorius, J.G.M. Winkelman, A.A.C.M. Beenackers, Chem. Eng. Sci. 56 (2001) 547.
[5] R. Molinari, M. Mungari, E. Dorioli, A.S. Paola, V. Loddo, L. Palmisano, M. Schiavello, Catal. Today 55 (2000) 71.
[6] T. Tsuru, T. Toyosada, T. Yoshioka, M. Asaeda, J. Chem. Eng. Jpn. 34 (2001) 844.
[7] T. Tsuru, T. Toyosada, T. Yoshioka, M. Asaeda, J. Chem. Eng. Jpn., submitted for publication.
[8] F. Shiraishi, K. Toyoda, S. Fukinbara, E. Obuchi, K. Nakano, Chem. Eng. Sci. 54 (1999) 1547.
[9] E. Obuchi, T. Sakamoto, K. Nakano, F. Shiraishi, Chem. Eng. Sci. 54 (1999) 1525.
[10] S. Yamazaki-Nishida, K.J. Nagano, L.A. Philips, S. Cevera-March, M.A. Anderson, J. Photochem. Photobiol. A: Chem. 70 (1993) 95.
[11] M.A. Anderson, S. Yamazaki-Nishida, S. Cevera-March, in: D.F. Ollis, H. Al-Ekabi (Eds.), Photocatalytic Purification and Treatment of Water and Air, Elsevier, Amsterdam, 1993.
[12] C.S. Turchi, D.F. Ollis, J. Phys. Chem. 92 (1988) 6853.
[13] T. Tsuru, Sep. Purif. Meth. 30 (2001) 191–220.
[14] T. Tsuru, D. Hironaka, T. Yoshioka, M. Asaeda, Sep. Purif. Technol. 25 (2001) 441.
[15] T. Tsuru, T. Hino, T. Yoshioka, M. Asaeda, J. Membr. Sci. 186 (2001) 257.